ADVANCES IN ARCHITECTURE, PLANNING AND DESIGN

EDITOR

ASSOC. PROF. HÜSEYİN SAMET AŞIKKUTLU,PH.D

DOI:10.5281/zenodo.14582391

Advances in Architecture, Planning and Design

EDITOR

Assoc. Prof. Hüseyin Samet Aşıkkutlu ,Ph.D.

Publisher
Platanus Publishing®

Editor in Chief
Assoc. Prof. Hüseyin Samet Aşıkkutlu, Ph.D.

Cover & Interior Design
Platanus Publishing®

Editorial Coordinator
Arzu Betül Çuhacıoğlu

The First Edition
December, 2024

Publisher's Certificate No
45813

ISBN
978-625-6982-22-3

©copyright
All rights reserved. No part of this publication may be reproduced or transmitted in any form or by any means, electronic or mechanical, including photocopy, or any information storage or retrieval system, without permission from the publisher.

Platanus Publishing®
Address: Natoyolu Cad. Fahri Korutürk Mah. 157/B, 06480, Mamak, Ankara, Turkey.
Phone: +90 312 390 1 118
web: www.platanuskitap.com
e-mail: platanuskitap@gmail.com



PLATANUS PUBLISHING®

CONTENTS

CHAPTER 1 7

The Impact of Green Spaces in Mitigating the Urban Heat Island Effect: A Systematic Review of the Literature

Seyhan Seyhan & Halil Duymuş,&Mehtap Özenen Kavlak,& Alper Çabuk,

CHAPTER 2 39

Comparison of Machine Learning-Based and Spectral Index-Supported Image Classification Algorithms Using The Google Earth Engine (GEE) Platform

İsmail Yılmaz,& Serdar Selim

CHAPTER 3 59

Accommodation of Temporary Residents of Constructıin Sites an Evaluation of Workers' Barracks

Yavuz Arat& Merve Kanat İçöz

CHAPTER 4 85

Rethinking Image and Identity of the City: A Review

Beyza Onur

CHAPTER 5 95

Repurposing of Industrial Buıldıngs: An Assessment in the Context of Sustainability

Merve Tuna Kayılı

CHAPTER 6 117

Investigation of Land Use/Cover Changes After the Disease Pandemic Using Remote Sensing Technologies; the Case of Antalya Döşemealtı

Göktuğ Yaşar Çukurlu & Namık Kemal Sönmez & Mesut Çoşlu

CHAPTER 7 129

Determination of The Social Carrying Capacity of Günpınar Waterfall Nature Park in Malatya Province

Halit Koçak & Metin Demir

CHAPTER 8 149

A Multi-Criteria Analysis and Planning Strategies for Green Spaces in The City of Antalya
Ebru Manavoğlu & Veli Ortacesme

CHAPTER 9 169

Analysing Konya City Mevlâna Street in terms of Pedestrian Safety
Banu Öztürk Kurtaslan

CHAPTER 10..... 197

Evaluation of the Contribution of School Gardens to Ecosystem Services
Demet Ulkü Gülpınar Sekban

CHAPTER 11..... 213

A Multi-Faceted Evaluation of a Roof Garden with Different Approaches
Demet Ulkü Gülpınar Sekban

CHAPTER 12..... 225

Health-Oriented Interior Architecture Principles for Primary Care Centers (PCCs): Ergonomics, Air Quality, Lighting, and Acoustics
Mustafa Kucuktuvek & Hilal Tuğba Örmecioğlu

CHAPTER 13..... 241

Urban Living Labs: An Innovative Participation Tool for Smart City Development
Sinan Levend

CHAPTER 14..... 273

Examining the Concept of Therapeutic Landscape in terms of Human-Nature Relationship
Hilal Kahveci & Makbulenur Onur

CHAPTER 15..... 287

Landscape Character Types Determination on A National Scale
Rüya Yılmaz & Okan Yılmaz & Derya Serbest Şimşek

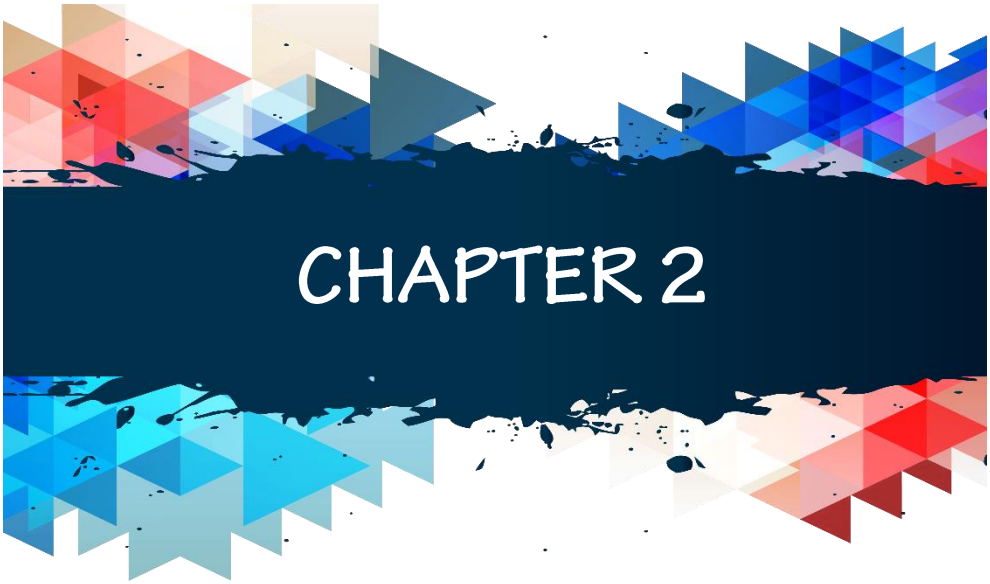
CHAPTER 16..... 302

Current Problems in Building Economy
Zubaidah Nadhem Mahmood Alzubaidiyazar Elif Sözer & Dilek Yasar

CHAPTER 17 320

Re-Functionalisation of Immovable Cultural Heritage: The Case of Niğde City

Nuriye Ebru Yıldız & Barış Kahveci



Comparison of Machine Learning-Based and Spectral Index-Supported Image Classification Algorithms Using The Google Earth Engine (GEE) Platform

İsmail Yılmaz[1,2]& Serdar Selim[3]

[1] PhD Student, Akdeniz University, Institute of Science, Department of Remote Sensing and Geographical Information Systems
[2] The Company of Smart City and Partners, Gold N State Plaza, 2673 Street. No:38/30 Çankaya, Ankara. ORCID: 0000-0001-7117-759X
[3] Assoc. Prof. Dr, Akdeniz University, Faculty of Science, Department of Space Science and Technologies. ORCID: 0000-0002-5631-6253, Corresponding Author

1. Introduction

Advancements in remote sensing and satellite imagery have made land use and land cover (LULC) mapping via automated image classification a critical research topic (Balha et al., 2021; Selim et al., 2023). This is because LULC changes are phenomena that impact ecological, economic, social, and cultural parameters, influencing societal well-being, development, the sustainability of global resources, and climate variability (Wang et al., 2022; Cinar et al., 2023; Karakuş et al., 2024). Automated image classification is among the most convenient and widely preferred techniques for generating LULC maps of a given area (Talukdar et al., 2020).

LULC classes are generated by classifying pixels with similar values across multiple image bands through digital image classification techniques. Common approaches include object-based, supervised, and unsupervised methods. Object-based classification primarily uses image segmentation algorithms to group spectrally homogeneous pixels into image objects, which are then classified individually (Liu and Xia, 2010). Supervised classification relies on the concept of a user selecting sample pixels that represent specific classes in an image, allowing image processing software to use these training sites as references to classify all other pixels in the image (Carrizosa and Morales, 2013). Unsupervised classification techniques, which lack a training phase, are generally more efficient and faster to implement. Conventional unsupervised classification methods use user-defined parameters, such as the number of classes, stopping criteria, or algorithm iterations. A primary challenge is determining optimal values for these parameters to achieve satisfactory classification results (Matci and Avdan, 2020). Numerous scientific studies in the literature have aimed to identify the best-performing classification algorithm by comparing different methods (Balha et al., 2021; Chughtai et al., 2021; Naushad et al., 2021; Basheer et al., 2022; Krivoguz et al., 2023). Some of these classification algorithms include Minimum Distance (MD), Maximum Likelihood (ML), Fuzzy Classification (FC), Artificial Neural Network (ANN), Support Vector Machine (SVM), Random Forest (RF), Deep Learning (DL), Deep Transfer Learning (DTL), and Light Gradient Boosting Machine (LightGBM). These studies have utilized various Geographic Information System (GIS)-based software, both proprietary (e.g., ENVI, ERDAS Imagine, and ArcGIS) and open-source (e.g., QGIS, GEE). One such platform, Google Earth Engine (GEE), is a web-based platform that enables access to a vast repository of satellite images, facilitating global analysis and visualization. GEE offers open access to extensive datasets, including satellite image archives, making it a valuable resource for scientists and

researchers conducting geospatial and remote sensing analyses (Avcı et al., 2023).

The innovation of this study lies in testing the SVM, RF, and LightGBM algorithms to produce an LULC map of a region using entirely open-source, freely accessible software and data, and comparing the results with the latest Esri LULC map. To improve classification outcomes, the study incorporates the Normalized Difference Vegetation Index (NDVI), Normalized Difference Water Index (NDWI), and Normalized Difference Built-up Index (NDBI) into the classification process. Additionally, the study area is subject to rapid LULC change due to tourism pressure, rapid urbanization, and frequent wildfire events. Therefore, generating a high-accuracy, practical LULC map for this region holds particular importance.

2. Study area

Located within the borders of the Mediterranean Region in southern Turkey, Antalya is a significant hub for both tourism and agriculture (Olgun et al., 2024). The district of Kemer in Antalya, one of Turkey's most significant tourism destinations, was selected as the study area. Located on a 46 km coastal strip at the foothills of the Western Taurus Mountains, Kemer is positioned at coordinates 36°36'7.23"N and 30°33'28.47"E (Figure 1). The district, bordered by the Mediterranean Sea to the east and forests and mountains to the west, covers an area of 53.483 km², with 45,000 hectares of forest land. The climate is hot and dry in summer, mild and rainy in winter, and the highest elevation in the district center is 15 meters. On average, Kemer enjoys 300 sunny days per year. The district's population was 46,143 in 2019 (Kemer Municipality, 2024), and as of 2024, this figure is approximately 50,000.

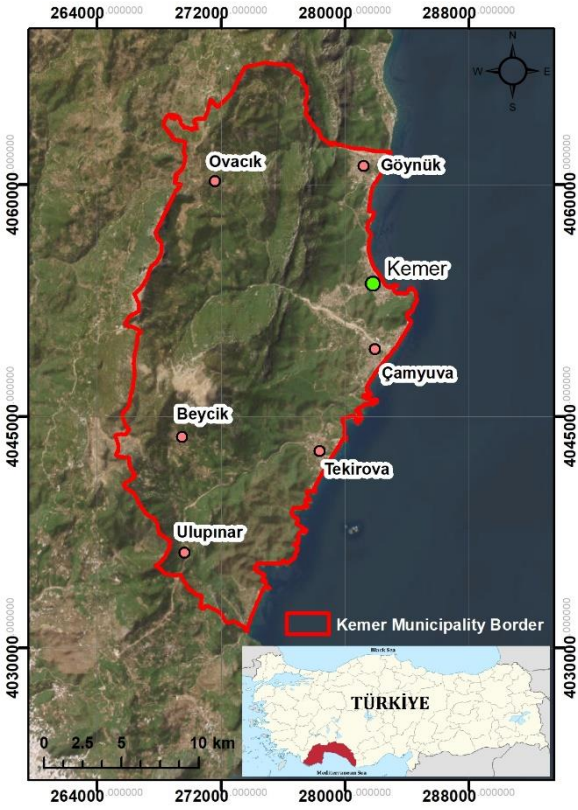


Figure 1. Location of the study area

The district's vegetation consists primarily of maquis formations, typical of the Mediterranean region, along with a belt of Red Pine (*Pinus brutia*) forests. Coastal settlements, such as Göynük, Çamyuva, and Tekirova, host a significant portion of the population, while the interior areas feature village settlements.

3. Data sets

The primary dataset for this study comprises a Sentinel-2 satellite image of the region from June 19, 2024, with a 10-meter spatial resolution and open access, along with a 10-meter annual map of Earth's land surface from 2023 obtained from ArcGIS Living Atlas of the World. The approximate one-year gap between the two images was disregarded. The up-to-date Sentinel-2 satellite image was sourced from https://browser.dataspace.copernicus.eu/, and the Esri LULC map was obtained from https://livingatlas.arcgis.com/landcoverexplorer. This LULC map is reported to be developed with Artificial Intelligence (AI) support using a training dataset of billions of human-labeled image pixels (ESRI, 2024a). The resulting nine-class surface map includes categories such as crops, water, bare

surface, vegetation types, and built areas. For the specific study area, five distinct land classes (range land, built area, crops, trees, and water) were defined for both maps.

4. Methods

The study methodology consists of four steps after data preprocessing (including radiometric correction and projection definition): application of classification algorithms, incorporation of spectral indices into the model, accuracy assessment and comparison.

4.1 Supervised Classification algorithms

In supervised classification, the user specifies various pixel values or spectral signatures that should be associated with each class. This is done by selecting representative sample areas of a specific land cover type to create a training dataset. The software algorithm then uses the spectral signatures from these training areas to classify the entire image. Ideally, classes should overlap with each other as little as possible. In this study, commonly preferred and recommended machine learning based algorithms in the literature, such as SVM, RF, and LightGBM, were employed (Talukdar et al., 2020; Ardahanlıoğlu et al., 2020; Bui et al., 2021; Babitha et al., 2023; Li et al., 2024).

4.1.1 Suppor Vector Machine (SVM): One of the machine learning techniques, SVM, aims to not only maximize the margin of separation between different boundaries but also minimize the error. SVM can also be applied in supervised learning techniques for regression models (Vapnik, 1999). Using the SVM classifier offers several advantages (Prasad et al., 2017). The SVM classifier does not require samples to be regularly distributed and needs fewer samples. It is less likely to be affected by noise, correlated bands, or an uneven number or size of training sites within each class (ESRI, 2024b).

4.1.2 Random Forest (RF): The random forest, also known as the random tree's classifier, is a method for classifying images that can handle segmented images and other supplementary raster datasets and is resistant to overfitting (ESRI, 2024b). The Random Forest is composed of several decision trees, each of which will grow fully, does not require processing to be cut, produces more accurate results, and does not overfit. With its automatic feature selection and other benefits, the random forest algorithm will perform the total estimate (Lin et al., 2017). RF has become one of the most popular options for LULC mapping because of its improved accuracy and efficiency, cheap computational cost, and requirement for only a few parameters (Amini et al., 2022).

4.1.3 Light Gradient Boosting Machine (LightGBM): For categorization challenges, a number of potent machine learning algorithms based on decision trees have recently been created. A relatively new method called Light Gradient Boosting Machine (LightGBM) has gained popularity due to its exceptional performance in machine learning competitions. These innovative machine learning algorithms are expansions of traditional ensemble boosting methods from the Classification and Regression Tree family (Abdi, 2020). Despite being a fairly basic algorithm, its exceptional performance and adaptability have made it one of the most popular nonlinear algorithms (Liang et al., 2021). In contrast to the random forest technique, LightGBM is a tree ensemble approach that generates one regression tree at a time by fitting the residuals of the trees that came before it. This process is known as boosting (Candido et al., 2021). LightGBM is relatively fast and has low memory usage, and is designed to provide high speed on large data while providing high accuracy even on small data samples (Ahn et al., 2023).

4.2 Spectral indices

Spectral indices are commonly used to facilitate the LULC mapping process and improve accuracy (Selim et al., 2022). A spectral index can be calculated using two or more bands from remotely sensed satellite images (Eyileten et al., 2022). An index indicates the abundance of a specific class in the image (Santhosh and Shilpa, 2023). To better distinguish land classes and the LULC structure of the region in the study area, spectral indices such as NDVI for green areas, NDBI for built-up areas, and NDWI for water bodies have been incorporated into the model.

4.2.1 Normalized Difference Vegetation Index (NDVI): Because it is less sensitive to soil and atmospheric factors, the NDVI is a useful indicator for regions with medium to high vegetation densities. The index values, which vary from -1 to +1, are determined by how well healthy plants reflect infrared wavelengths and how poorly they reflect in the presence of the electromagnetic spectrum's red band. Consequently, greater NDVI values are typically associated with healthy forest cover (da Silva et al., 2020). Due to the region's dense vegetation, this index has been preferred to better distinguish forested areas from other classes. The NDVI formula is provided in Equation (1) (Piragnolo et al., 2018).

$$NDVI = \frac{NIR-Red}{NIR+Red} \quad (1)$$

In equation (1), NIR refers to band 8 and Red refers to band 4 for the Sentinel 2 satellite images.

4.2.2 Normalized Difference Built-up Index (NDBI): Buildings, roads, and other infrastructure, such as bridges and pavements, are considered by the widely used NDBI, mainly the impervious cover (Keerthi Naidu and Chundeli, 2023). The built-up area of urban land is extracted using the normalized difference built-up index (NDBI). The range of the NDBI value is-1.0 to +1.0. Built-up area is indicated by a greater NDBI value, water bodies are indicated by a negative value, and vegetation is indicated by a lower value. A larger positive value of the built-up index indicates areas that are built up and areas that are desolate. Both cultivated and uncultivated land are extracted using this index (Pokhariya et al., 2023). NDBI formula is provided in Equation (2) (Duan et al., 2019).

$$NDBI = \frac{SWIR-NIR}{SWIR+NIR} \quad (2)$$

Bands 8 and 11 of the Sentinel-2 data represent NIR and SWIR, respectively.

4.2.3 Normalized Difference Water Index (NDWI): The NDWI highlights the water and glacial cover in a satellite picture by using values from the green and near-infrared (NIR) spectral bands. Water, snow, and ice are represented by positive numbers on the index, which goes from -1 to 1. Soil and terrestrial plants are represented by values smaller than zero (Hamid et al., 2024). Also, the NDWI is used to track variations in aquatic bodies' water content. NDWI highlights water bodies using green and near-infrared bands because water bodies absorb a lot of light in the visible to infrared electromagnetic spectrum (Gao et al., 1996). NDWI formula is provided in Equation (3) (Roy et al., 2024).

$$NDWI = \frac{Green-NIR}{Green+NIR} \quad (3)$$

Bands 3 and 8 of the Sentinel-2 data represent Green and NIR, respectively. The NDWI index has been used in this study to clearly distinguish the boundary between land and water, as well as to identify areas with high water content in terrestrial regions.

4.3 Accuracy Assessment

One important stage in processing data from remote sensing is accuracy assessment. For a user, it determines the information value of the generated data.

Only when the quality of the data is known can geodata be used productively. Each pixel's classification is compared to the specific land cover conditions derived from the associated ground truth data to determine the overall correctness of the categorized image. Errors of omission, a gauge of how accurately real-world land cover categories may be categorized, are measured by producer accuracy. Errors of commission, which indicate the probability that a classified pixel would match the kind of land cover of its corresponding real-world location, are measured by the user's accuracy (Rwanga and Ndambuki, 2017).

To perform accuracy analysis of the classified images, the map was first divided into grids of 1 km x 1 km, and an automatic point was assigned to the center of each grid. The reflectance values of the pixels corresponding to these points were then extracted and compared with current Google Earth satellite images. In this context, kappa coefficient and overall accuracy were generated on the GEE platform. The kappa coefficient and error matrix are now commonly used to evaluate the accuracy of image classification.

4.3 Comparison of classified images with LULC from Earth's land surface

In the final stage of the study, the overall accuracy and kappa coefficients of three different classified satellite images, supported by spectral indices, were compared with the overall accuracy and kappa values of ESRI's AI-assisted LULC map. This comparison was made to test the usability of all classified images and ESRI Land Cover maps, which display global land cover classes, in various planning studies. Based on accuracy values, the classification algorithms were ranked for the specific study area.

5. Results

This study, conducted in the Kemer district, which has a dynamic LULC structure under the pressure of rapid urbanization and population growth, utilized freely available satellite images and user-friendly, open-access software. The aim of the study was to achieve the highest accuracy by supporting different machine learning based classification techniques with spectral indices in a fast and practical manner. The maps produced through supervised classifications were compared with the AI-assisted ESRI Land Cover map, and their accuracies were evaluated.

5.1. Results of spectral index supported classification algorithms

The NDVI, NDBI, and NDWI indices were applied to Sentinel-2 satellite images, with vegetation, artificial surfaces, and areas with high water content being primarily identified (Figure 2). The study area is predominantly covered by

dense forest vegetation. From the coastal zone to the higher altitudes, both dense and sparse vegetation cover dominate the area. Artificial surfaces are mainly concentrated along the coast, and small settlements around east-west transportation routes are separated from other land cover classes using the NDBI. The NDWI, on the other hand, effectively delineated the coastline, distinguishing areas with high moisture content from completely dry areas.

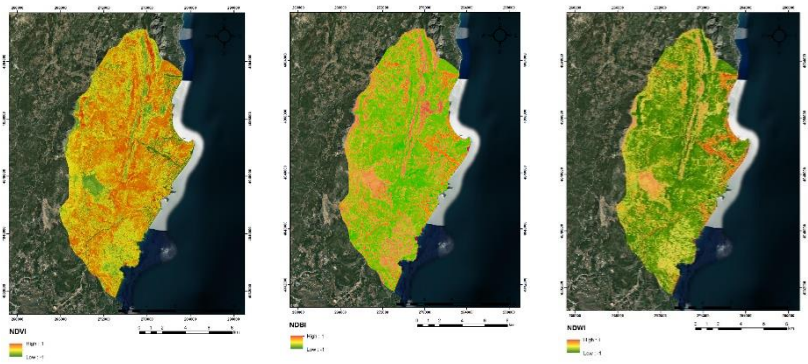


Figure 2. NDVI (left), NDBI (middle), NDWI (right) maps

In the NDVI map, red tones indicate dense vegetation, while green tones represent sparse vegetation with lower NDVI values. In the NDBI map, red tones depict areas of dense urbanization or artificial surfaces, while green tones represent natural areas. In the NDWI map, red colors represent water surfaces and areas with high moisture content, whereas green tones indicate areas with little or no water.

The maps produced using spectral indices were incorporated as input data into the GEE platform for supervised classification, and classification processes were carried out. In the SVM map, data points in the feature space were effectively separated into different classes (Figure 3). In particular, artificial surfaces were effectively distinguished from other classes with the support of spectral index inputs.

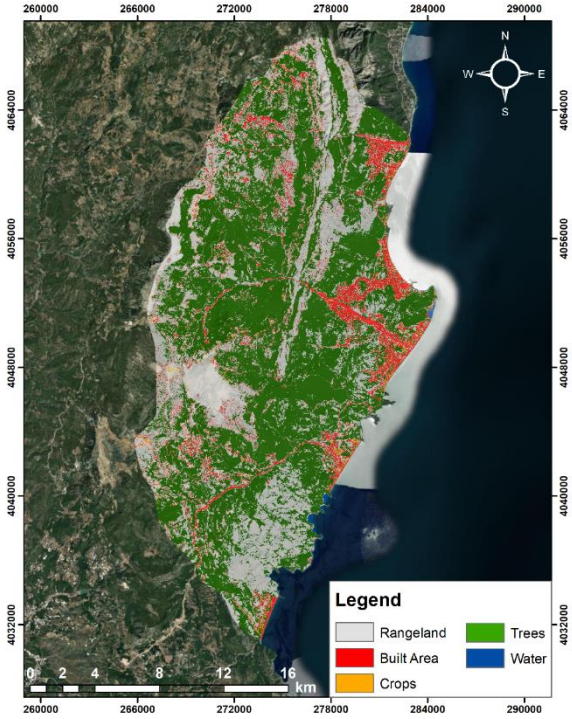


Figure 3. SVM map

In the RF map, the built area has been classified in a more fragmented structure. The tree class and the rangeland class appear to be interwoven in many different areas (Figure 4).

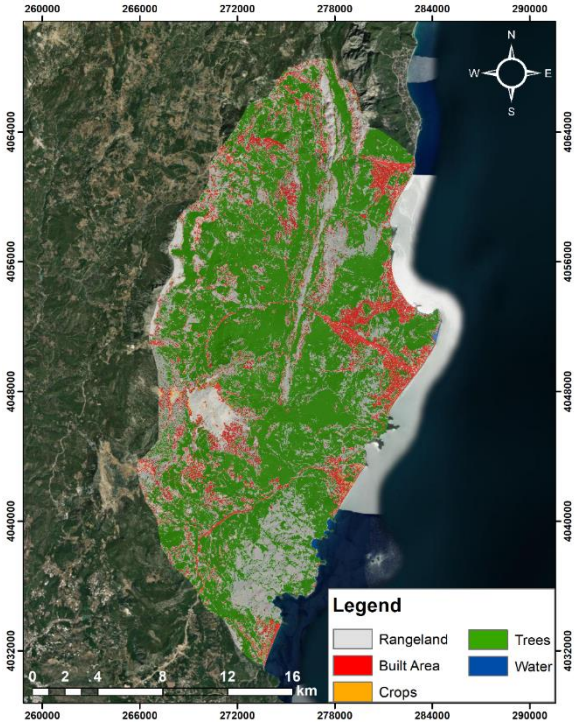


Figure 4. RF map

In the classification created with the LightGBM algorithm, the trees class occupies a larger area compared to the other classes. The built area is more structured compared to the RF classification. The rangeland class is also clearly separated from the other classes (Figure 5).

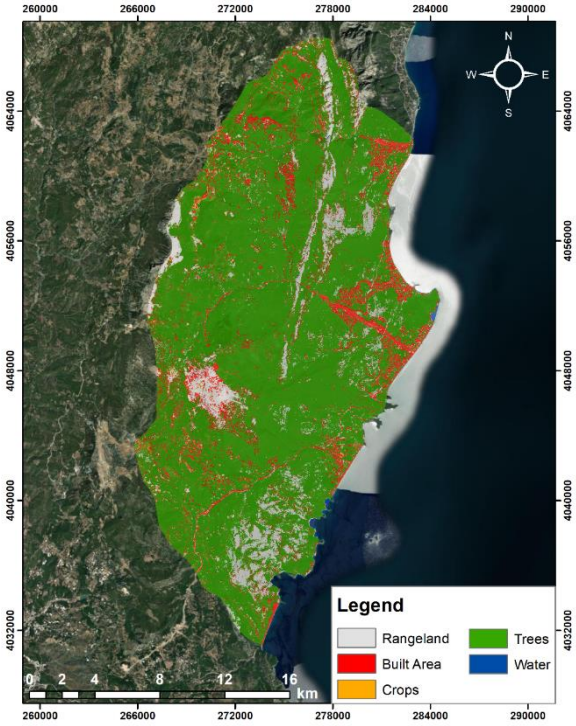


Figure 5. LightGBM map

In the image where three different classification algorithms were applied, it was observed that all classes were systematically separated. Specifically, the built area and rangeland classes were distinctly separated in all classifications. However, when comparing the classification processes of the algorithms, differences were noted, with some algorithms performing better for certain classes while others were less effective.

5.2. Comparison of classification results with ESRI LULC and accuracy assessment

ESRI's AI-assisted classification model generates an LULC map by classifying land surfaces at a 10-meter resolution. This map is created by aggregating a vast number of training datasets from six spectral bands. In the scope of the study, the image, which was subset according to land boundaries, shows a clear distinction between all classes (Figure 6). The settlement areas along the coast and the built-up areas in the interior regions are quite prominent in this map. Furthermore, the boundaries of the rangeland and crops classes are more distinct compared to other classification algorithms. The coastline in this LULC map also clearly separates the land surface from the water surface.

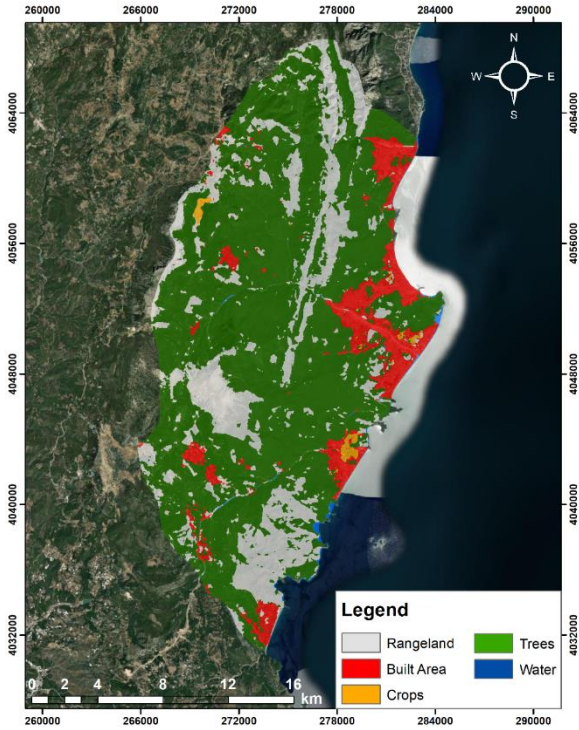


Figure 6. ESRI LULC map

When all the produced maps are evaluated in terms of LULC classes, the results shown in Table 1 are obtained.

Table 1. Class area values of all classification algorithms

Area (km²)	**SVM**	**LightGBM**	**RF**	**ESRI LULC**
Rangeland	150,44	44,86	144,02	92,89
Built area	33,02	45,38	46,22	37,23
Trees	223,87	320,41	216,95	277,30
Water	1,00	0,92	1,01	1,86
Crops	4,83	1,59	4,96	2,53
total	413,18	413,18	413,18	411,83

In all classifications, forest areas cover the largest area. The LightGBM algorithm produces the highest value with 320,41 km², while the RF algorithm gives the lowest value with 216,95 km². The ESRI LULC map provides an intermediate value of 277,30 km² for the same class. For the rangeland class, SVM and RF generate similar results, with areas of 150,44 km² and 144,02 km²,

respectively. The ESRI data for this class has a value of 92,89 km². In the built area class, both the LightGBM and RF algorithms yield areas of approximately 45-46 km², while SVM produces around 33 km², and the ESRI data provides a value of 37,23 km². For the water class, the ESRI data reports 1,86 km², while all other classification algorithms produce similar results of around 1 km². In the crops class, SVM and RF generate values of 4,83 km² and 4,96 km², respectively, while ESRI reports 2,53 km², with LightGBM producing the closest result at 1,59 km².

The accuracy of the classifications performed for the study area was compared with current Google Earth satellite images. In the area divided into grids, the pixel value at the center of each grid was used to assess whether the classified image overlapped with the actual land cover. The resulting accuracy assessment is shown in Table 2.

Table 2. Accuracy levels of classifications

Classification Algorithms	Overall Accuracy (%)	Kappa Statistic
ESRI LULC	84,52	0,70
LightGBM	75,24	0,47
SVM	71,19	0,48
RF	67,62	0,44

According to Table 2, the highest overall accuracy and Kappa statistics are associated with the ESRI LULC dataset, with an overall accuracy of 84,52% and a Kappa value of 0,70. This dataset has been used as a reference point for classification accuracy and provides highly reliable results for the Kemer district. The algorithms following the ESRI LULC dataset are LightGBM with 75,24% overall accuracy and a Kappa value of 0,47; SVM with 71,19% accuracy and a Kappa value of 0,48; and the RF algorithm with 67,62% accuracy and a Kappa value of 0,44.

The accuracy values for each class in the supervised classification algorithms are shown in Table 3.

Table 3. Accuracy levels of classifications at class level

Classification algorithms	Rangeland (%)	Built area (%)	Crops (%)	Trees (%)	Water (%)
ESRILULC	73,08	88,89	56,25	89,86	100
LightGBM	33,65	66,67	12,5	94,57	100
SVM	50,33	31,03	12,5	91,59	100
RF	64,42	72,22	6,25	71,38	100

According to Table 3, overall, the ESRI LULC dataset provides very high accuracy for all classes. Compared to other classification algorithms, the accuracy level in the trees class is only lower than that of LightGBM and SVM; however, the difference is within an acceptable range. The fragmentation of agricultural areas into small patches across the land and the fact that a large portion of these areas is fragmented around settlements significantly reduced the classification accuracy for this class. Additionally, the crops class has mixed with the tree class in many areas. Despite this, the ESRI LULC dataset provided significant accuracy in this class compared to other algorithms. For the rangeland class, after the ESRI LULC dataset, the highest accuracies were achieved by RF, SVM, and LightGBM, respectively. In the built area class, SVM showed the lowest performance. In the crops and tree classes, both LightGBM and SVM reached very high accuracy, demonstrating excellent performance. For the water class, all classification algorithms achieved very high accuracy.

6. Discussion and Conclusion

Land cover mapping is essential for many applications, including urban planning, environmental management, and natural resource management, as it provides critical information. Specifically, the widespread availability of time-series satellite imagery and the development of digital image processing have made it possible to observe, track, assess, and understand the temporal and spatial fluctuations in land cover (Wang et al., 2018; Candido et al., 2021). In this study, which tested different machine learning based classification algorithms for LULC in the Kemer district, it was found that the AI-supported ESRI LULC dataset achieved higher accuracy compared to SVM, LightGBM, and RF algorithms. Given the rapid changes in land cover due to various anthropogenic factors, the ESRI LULC dataset, with its ease of accessibility, minimal expertise requirements, and high accuracy, can assist central and local governments in decision-making processes. In terms of overall accuracy and kappa statistics, LightGBM, SVM, and RF were ranked after ESRI LULC based on their accuracy

levels. While LightGBM outperformed the other implemented classification algorithms, its significant disadvantage is the large number of hyperparameters it requires (Ke et al., 2017). The literature states that LightGBM is preferred over RF because it is newer, faster, and more successful (McCarty et al., 2020). Although the processing time required to apply LightGBM is longer, the results confirmed its superiority over other popular machine learning algorithms such as RF and SVM (McCarty et al., 2020; Liang et al., 2021). In this study, LightGBM showed better performance than RF. However, for the rangeland class, LightGBM performed the worst compared to other classification algorithms. This is likely because rangeland and tree classes have similar spectral reflectance, which the algorithm could not clearly differentiate. The SVM algorithm, on the other hand, showed the lowest performance in the built area class. Also, the literature suggests that RF may perform better than SVM in built-up class for LULC classification (Talukdar et al., 2020; Avcı et al., 2023).

Finally, while nearly all classifications showed maximum performance for the water class, they performed poorly for the crops class. This is likely due to the similar spectral reflectance between the crops and trees classes. Therefore, when performing crops classification, it is recommended to include a greater number of samples in the classification and to divide the crops class into sub-classes (based on agricultural crop patterns) for the algorithms to work more effectively.

The results of this study show that the ESRI LULC classes provided higher accuracy compared to other machine learning classification algorithms for the study area. Therefore, due to its availability, ease of access, minimal expertise requirements, suitability for use over large areas, and high accuracy, it can be preferred as a reference dataset in planning decisions.

References

Abdi, A. M. (2020). Land cover and land use classification performance of machine learning algorithms in a boreal landscape using Sentinel-2 data. GIScience & Remote Sensing, 57(1), 1-20.

Ahn, J. M., Kim, J., & Kim, K. (2023). Ensemble machine learning of gradient boosting (XGBoost, LightGBM, CatBoost) and attention-based CNN-LSTM for harmful algal blooms forecasting. Toxins, 15(10), 608.

Amini, S., Saber, M., Rabiei-Dastjerdi, H., & Homayouni, S. (2022). Urban land use and land cover change analysis using random forest classification of landsat time series. Remote Sensing, 14(11), 2654.

Ardahanlıoğlu, Z. R., Selim, S., Karakuş, N., & Çınar, İ. (2020). GIS-based approach to determine suitable settlement areas compatible with the natural environment. 23(1), 71-82.

Avcı, C., Budak, M., Yağmur, N., & Balçık, F. (2023). Comparison between random forest and support vector machine algorithms for LULC classification. International Journal of Engineering and Geosciences, 8(1), 1-10.

Babitha, M. S., Andrushia, A. D., & Mehthab, A. (2023). A Comparative Analysis of Gradient Boost Algorithm and Deep Neural Network for Land Cover Land Use Classification. In 2023 9th International Conference on Smart Computing and Communications (ICSCC) (pp. 18-24). IEEE.

Balha, A., Mallick, J., Pandey, S., Gupta, S., & Singh, C. K. (2021). A comparative analysis of different pixel and object-based classification algorithms using multi-source high spatial resolution satellite data for LULC mapping. Earth Science Informatics, 14(4), 2231-2247.

Basheer, S., Wang, X., Farooque, A. A., Nawaz, R. A., Liu, K., Adekanmbi, T., & Liu, S. (2022). Comparison of land use land cover classifiers using different satellite imagery and machine learning techniques. Remote Sensing, 14(19), 4978.

Bui, Q. T., Chou, T. Y., Hoang, T. V., Fang, Y. M., Mu, C. Y., Huang, P. H., ... & Meadows, M. E. (2021). Gradient boosting machine and object-based CNN for land cover classification. Remote Sensing, 13(14), 2709.

Candido, C., Blanco, A. C., Medina, J., Gubatanga, E., Santos, A., Ana, R. S., & Reyes, R. B. (2021). Improving the consistency of multi-temporal land cover mapping of Laguna lake watershed using light gradient boosting machine (LightGBM) approach, change detection analysis, and Markov chain. Remote Sensing Applications: Society and Environment, 23, 100565.

Carrizosa, E., & Morales, D. R. (2013). Supervised classification and mathematical optimization. Computers & Operations Research, 40(1), 150-165.

Chughtai, A. H., Abbasi, H., & Karas, I. R. (2021). A review on change detection method and accuracy assessment for land use land cover. Remote Sensing Applications: Society and Environment, 22, 100482.

Cinar, İ., Karakuş, N., & Toy, S. (2023). Analysing daytime summer thermal comfort conditions for Turkey's third largest tourism destination. Environmental Science and Pollution Research, 30(17), 50046-50056.

da Silva, V. S., Salami, G., da Silva, M. I. O., Silva, E. A., Monteiro Junior, J. J., & Alba, E. (2020). Methodological evaluation of vegetation indexes in land use and land cover (LULC) classification. Geology, Ecology, and Landscapes, 4(2), 159-169.

Duan, Q., Tan, M., Guo, Y., Wang, X., & Xin, L. (2019). Understanding the spatial distribution of urban forests in China using Sentinel-2 images with Google Earth Engine. Forests, 10(9), 729.

ESRI, (2024a). ESRI Land Cover, https://livingatlas.arcgis.com/landcover/ (accessed date: 30.10.2024).

ESRI, (2024b). Train Support Vector Machine Classifier in Spatial Analyst, https://pro.arcgis.com/ (accessed date: 30.10.2024).

Eyileten, B., Esendağlı, Ç., & Selim, S. (2022). Assessment of urban green space distribution within the scope of European green deal using NDVI indice; case of Nicosia/Cyprus. Journal of Architectural Sciences and Applications, 7(2), 615-623.

Gao, B. C. (1996). NDWI—A normalized difference water index for remote sensing of vegetation liquid water from space. Remote sensing of environment, 58(3), 257-266.

Hamid, I., Dar, L. A., & Akintug, B. (2024). Assessing land use land cover change using remote sensing and GIS techniques: A case study of Kashmir Valley. Journal of Earth System Science, 133(3), 1-17.

Karakuş, N., Selim, S., Selim, C., Olgun, R., Koç, A., Ardahanlıoğlu, Z. R., Şenyiğit Doğan, S., & Ertoy, N. (2024). Evaluation of Thermal Comfort Conditions in the Working Environments of Seasonal Agricultural Workers in Csa Koppen Climate Type. Sustainability, vol.16, no.20, 1-18.

Ke, G., Meng, Q., Finley, T., Wang, T., Chen, W., Ma, W., ... & Liu, T. Y. (2017). Lightgbm: A highly efficient gradient boosting decision tree. Advances in neural information processing systems, 30.

Keerthi Naidu, B. N., & Chundeli, F. A. (2023). Assessing LULC changes and LST through NDVI and NDBI spatial indicators: A case of Bengaluru, India. GeoJournal, 88(4), 4335-4350.

Kemer Municipality (2024). Official website of Kemer Municipality, https://www.kemer.bel.tr/tr/tarihcemiz (accessed date: 30.10.2024).

Krivoguz, D., Chernyi, S. G., Zinchenko, E., Silkin, A., & Zinchenko, A. (2023). Using Landsat-5 for accurate historical LULC classification: A comparison of machine learning models. Data, 8(9), 138.

Li, R., Gao, X., & Shi, F. (2024). A Framework for Subregion Ensemble Learning Mapping of Land Use/Land Cover at the Watershed Scale. Remote Sensing, 16(20), 3855.

Liang, L., Hu, W., Zhang, Y., Ma, K., Gu, Y., Tian, B., & Li, H. (2021). An algorithm with LightGBM+ SVM fusion model for the assessment of dynamic security region. In E3S Web of Conferences (Vol. 256, p. 02022). EDP Sciences.

Lin, W., Wu, Z., Lin, L., Wen, A., & Li, J. (2017). An ensemble random forest algorithm for insurance big data analysis. Ieee access, 5, 16568-16575.

Liu, D., & Xia, F. (2010). Assessing object-based classification: advantages and limitations. Remote sensing letters, 1(4), 187-194.

Matci, D. K., & Avdan, U. (2020). Optimization-based automated unsupervised classification method: A novel approach. Expert Systems with Applications, 160, 113735.

McCarty, D. A., Kim, H. W., & Lee, H. K. (2020). Evaluation of light gradient boosted machine learning technique in large scale land use and land cover classification. Environments, 7(10), 84.

Naushad, R., Kaur, T., & Ghaderpour, E. (2021). Deep transfer learning for land use and land cover classification: A comparative study. Sensors, 21(23), 8083.

Olgun, R., Karakuş, N., Selim, S., & Eyileten, B., (2024). Assessment and mapping of noise pollution in recreation spaces using geostatistic method after COVID-19 lockdown in Turkey. Environmental Science and Pollution Research, vol.31, no.23, 33428-33442.

Piragnolo, M., Lusiani, G., & Pirotti, F. (2018). Comparison of vegetation indices from RPAS and Sentinel-2 imagery for detecting permanent pastures. The International Archives of the Photogrammetry, Remote Sensing and Spatial Information Sciences, 42, 1381-1387.

Pokhariya, H. S., Singh, D. P., & Prakash, R. (2023). Evaluation of different machine learning algorithms for LULC classification in heterogeneous landscape by using remote sensing and GIS techniques. Engineering Research Express, 5(4), 045052.

Prasad, S. V. S., Savithri, T. S., & Krishna, I. V. M. (2017). Comparison of accuracy measures for RS image classification using SVM and ANN classifiers. International Journal of Electrical and Computer Engineering, 7(3), 1180.

Roy, K. C., Soren, D. D. L., & Biswas, B. (2024). Land-use/cover change and future prediction by integrating the ML techniques of random forest and CA-Markov chain model of the Ganges alluvial tract of Eastern India. Environment, Development and Sustainability, 1-28.

Rwanga, S. S., & Ndambuki, J. M. (2017). Accuracy assessment of land use/land cover classification using remote sensing and GIS. International Journal of Geosciences, 8(04), 611.

Santhosh, L. G., & Shilpa, D. N. (2023). Assessment of LULC change dynamics and its relationship with LST and spectral indices in a rural area of Bengaluru district, Karnataka India. Remote Sensing Applications: Society and Environment, 29, 100886.

Selim, S., Dönmez, B., & Kilçik, A. (2023). Determination of the optimum number of sample points to classify land cover types and estimate the contribution of trees on ecosystem services using the I-Tree Canopy tool. Integrated Environmental Assessment and Management, 19(3), 726-734.

Selim, S., Esendağlı, Ç., & Dönmez, B. (2022). Comparison of Different Indices Used for Shoreline Extraction from Landsat 8 Operational Land Imager in the context of Coastal Planning. In Recent Studies in Planning and Design (pp. 3-24). IK-SAD International Publishing House.

Talukdar, S., Singha, P., Mahato, S., Pal, S., Liou, Y. A., & Rahman, A. (2020). Land-use land-cover classification by machine learning classifiers for satellite observations—A review. Remote sensing, 12(7), 1135.

Vapnik, V. N. (1999). An overview of statistical learning theory. IEEE transactions on neural networks, 10(5), 988-999.

Wang, J., Bretz, M., Dewan, M. A. A., & Delavar, M. A. (2022). Machine learning in modelling land-use and land cover-change (LULCC): Current status, challenges and prospects. Science of The Total Environment, 822, 153559.

Wang, W., Li, W., Zhang, C., & Zhang, W. (2018). Improving object-based land use/cover classification from medium resolution imagery by Markov chain geostatistical post-classification. Land, 7(1), 31.